Energy Advances

ROYAL SOCIETY OF CHEMISTRY

PAPER

View Article Online
View Journal | View Issue

Cite this: *Energy Adv.*, 2022, 1, 900

Predictive energetic tuning of quinoid O-nucleophiles for the electrochemical capture of carbon dioxide†

Abdulaziz W. Alherz, ‡[bc] Haley A. Petersen, ‡[a] Nicholas R. Singstock, [b] Sohan N. Sur,[a] Charles B. Musgrave*[bd] and Oana R. Luca *[a]

The need for robust, scalable methods for the capture and storage of carbon dioxide is increasingly pressing. Electric power-based carbon capture methods have drawn attention as a promising strategy due to their potential to couple to renewable energy sources. Materials for the capture of CO_2 from air need to overcome the challenges of parasitic reactivity with oxygen, selective removal of CO_2 at 415 ppm, and long-term durability in air. Quinones and their reduced forms are a promising family of such sorbents. However, the design of robust quinone sorbents has been limited, and no systematic study exists that unifies the relationship between reduction potential, binding free energy and the effect of CO_2 concentration on the average number of CO_2 molecules captured. Our work addresses this knowledge gap through a synergistic computational and experimental study of a family of electrochemically generated quinoid molecular sorbents for CO_2 capture with tunable redox chemistries. Our findings indicate that while quinones with reduction potentials positive of oxygen reduction exist, the O-nucleophiles generated at these potentials are weak CO_2 binders. Using microkinetic analysis to examine binding speciation, we identify sorbent candidates that bind one CO_2 molecule within a narrow potential window positive of oxygen reduction. This behavior is calculated to occur at CO_2 concentrations relevant to direct air capture. Additionally, while electron-rich quinones are found to generally bind two CO_2 units per quinone dianion with little variation across CO_2 concentrations relevant to carbon capture, weaker quinones generally exhibit lower stoichiometries and are more sensitive to CO_2 concentration. Furthermore, we establish a linear correlation between the second reduction potential of a quinone and the free energy of binding CO_2 to the quinone dianion. This correlation has important predictive power, as it allows new molecular materials of the quinoid family to be assessed with simple electrochemical measurements. However, based on our findings, such analyses must be punctuated by careful considerations of reaction stoichiometry and operating concentration ranges.

Received 19th May 2022,
Accepted 26th September 2022

DOI: 10.1039/d2ya00114d

rsc.li/energy-advances

Introduction

Accumulation of CO_2 in the atmosphere has sparked an urgency in the development of methods for the capture and storage of CO_2.[1,2] While amine or aqueous sorbents of CO_2 are common, they require release steps with thermal swings and are more often used near concentrated emission sources.[3,4] These capture mechanisms are commonly not compatible with capture from a dilute source such as air and cannot be deployed in a dispersed, decentralized fashion.[5]

An analysis of CO_2 binding energetics for direct air capture reveals that sorbents for the capture of CO_2 do not need to be particularly strong CO_2 binders for applications that involve "skimming" small amounts of CO_2 from a stream rather than seeking complete CO_2 removal.[6]

Carbon capture using electrochemically generated species has attracted considerable attention in recent years due to its ability to couple with renewable power sources and the modularity of electrochemical devices.[3] Early work by Noble and coworkers[7] demonstrated that quinoid molecular sorbents can

[a] *Department of Chemistry, Materials Science and Engineering, and Renewable and Sustainable Energy Institute, University of Colorado Boulder, 215 UCB., Boulder, CO, 80309, USA. E-mail: oana.luca@colorado.edu*
[b] *Department of Chemical and Biological Engineering, University of Colorado, Boulder, CO 80309, USA. E-mail: charles.musgrave@colorado.edu*
[c] *Department of Chemical Engineering, College of Engineering and Petroleum, Kuwait University, P.O. Box 5969, Safat 13060, Kuwait*
[d] *Materials Science and Engineering Program, University of Colorado, Boulder, CO 80309, USA*

† Electronic supplementary information (ESI) available. See DOI: https://doi.org/10.1039/d2ya00114d

‡ These authors contributed equally.

be used to harvest CO_2 from dilute streams in nitrogen. More recently, Hatton and coworkers have demonstrated faradaic electroswing in an organic battery-like device in which quinones tethered to the electrodes are able to capture CO_2 when reduced and release it when oxidized.[8] In a related recent report, several quinones were categorized as strong *vs.* medium *vs.* weak binders of CO_2.[9]

In recent work from our group,[10] we identified an empirical linear correlation between the reduction potential necessary for the generation of a nucleophile and the nucleophile's ability to bind CO_2. Herein, we seek to extend this analysis to quinones due to their high importance in the field of reactive carbon capture. The equation of best fit from such a correlation can, in principle, be used to screen new quinoid molecules and to quickly estimate the free energy of binding of the electrogenerated nucleophile to CO_2. This can be achieved without CO_2 experiments and has a strong predictive value. We chose a subset of commercially available quinones that include electron poor quinones such as dichlorodicyanoquinone (DDQ), chloranil (4ClQ), 1,4-Dichloroquinone (2ClQ), and 1,2-dichloronaphthoquinone (2ClNQ). We hypothesized that a shift in the quinones' reduction potentials to potentials more positive than the reduction of oxygen would render sorbent systems impervious to O_2 degradation. Known strong binders such as reduced forms of benzoquinone (BQ), 1,5-dimethylbenzoquinone (2MeQ), and naphthoquinone (NQ) were also included as a comparison across a broader range of potentials. Cyclic voltammograms of 1 mM solutions of these quinones in acetonitrile at glassy carbon working electrodes are shown in Fig. 1. The quinones all exhibit the same reactivity pattern with two successive $1e^-$ reduction waves. Among the quinones screened, DDQ is most easily reduced (has the most positive reduction potential) and NQ is the most difficult to reduce (has the most negative reduction potential). Because species generated at more negative reduction potentials are more nucleophilic and therefore stronger CO_2 binders,[11,12] we expect the quinoid dianion nucleophiles generated from NQ to be the strongest binder of CO_2 in the series. The reduction potentials for the quinones listed above are provided in Table 1.

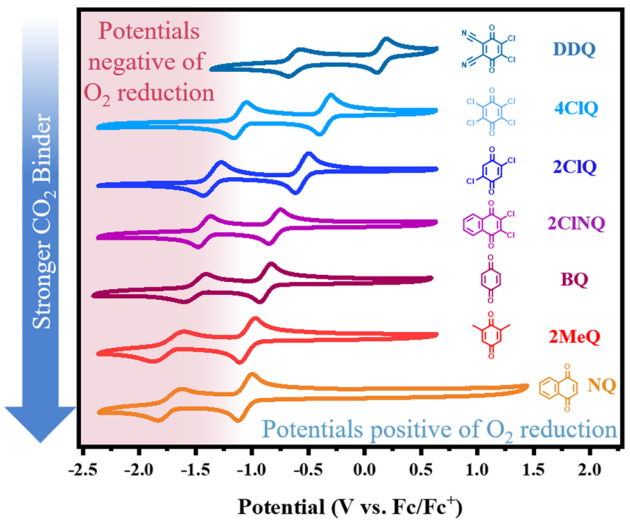

Fig. 1 Cyclic voltammetry of 1 mM solutions of quinone in MeCN with NBu_4PF_6 under Ar at 100 mV s^{-1}. Working electrode: glassy carbon; counter electrode: Pt wire; reference electrode: single-junction Ag electrode referenced externally *vs.* Fc/Fc^+.

With this potential ranking in hand, we proceeded to measure and quantify the free energy of CO_2 binding to establish the desired correlation. At the same time, we aimed to identify differences in reaction stoichiometry across the series, as this is an underexplored, yet critical topic. The goal of this work is to deliver a predictive tool for the estimation of CO_2 binding energies to electrochemically generated quinoid O-nucleophiles while carefully considering reaction stoichiometry.

Experimental determination of binding free energies

The strength of binding of an electroactive analyte to another species in solution can be determined electrochemically by monitoring the shift in potential of the corresponding electrochemical feature by CV. Similar analyses have been performed previously for association of reduced quinone species with ions in solution.[11,12] Creutz and coworkers used this analysis in their assessment of binding energies in reactions of CO_2 and metal centers.[13] In a related study, DuBois estimated binding constants to CO_2 for a small subset of reduced quinones using electroanalytical methods coupled to UV-Vis analysis and the Benesi–Hildebrand method.[14] Previous work by Nagaoka has also used similar methods to investigate the binding stoichiometry of weak binders.[15]

Electrochemical experiments for this study were conducted in acetonitrile (MeCN). MeCN was selected as a model polar aprotic solvent due to its minimal evaporation over the course of the experiment, high electrolyte solubility and thus high solution conductivity, and high CO_2 solubility. Protic solvents or additives are known to significantly affect the electrochemical responses of quinones due to hydrogen bonding or coupled protonation steps;[16] avoiding the use of protic solvents thus enables the evaluation of isolated reduction and CO_2 binding steps relevant to our analysis without concern of accompanying protonation steps. Although aqueous systems offer the advantages of lower volatility, low cost, and non-flammability, CO_2 solubility in neutral or acidic water is limited and suffers from the additional complication of carbonic acid equilibria. MeCN was hence selected as the optimal solvent for the present study, although recent work by Barlow and Yang has demonstrated the promising benefit of hydrogen-bonding stabilization by protic solvents of relevant quinone dianion and CO_2 adduct species.[17]

First, we define the reactions leading to the binding of CO_2 by the reduced quinone, given as follows:

$$Q + e^- \rightarrow Q^{\bullet -} \quad (1)$$

$$Q^{\bullet -} + e^- \rightarrow Q^{2-} \quad (2)$$

$$Q_2 + nCO_2 \overset{K}{\rightleftharpoons} \left(Q(CO_2)_n\right)^{2-} \quad (3)$$

A generic quinone, Q, first undergoes a single-electron reduction to generate the semiquinone radical anion, $Q^{\bullet -}$

Table 1 Experimental and DFT data for the family of quinones considered in this study

Entry	Stoichiometry Q^{2-}/CO_2[a]	DFT ΔG_{bind}[b]	Experimental ΔG_{bind}[bc]	Experimental uncertainty in ΔG_{bind}[bd]	DFT E_{red1}[e] (V)	DFT E_{red2}[e] (V)	Experimental E_{red1}[e] (V)	Experimental E_{red2}[e] (V)
DDQ	0[f]	3.1[g]	N/A	N/A	0.31	−0.95	0.12	−0.69
4ClQ	1	−4.90	−3.88	0.10	−0.27	−1.48	−0.40	−1.18
2ClQ	2	−8.90	−9.42	0.15	−0.48	−1.76	−0.62	−1.43
2ClNQ	1	−8.80	−5.00	0.25	−0.8	−1.91	−0.84	−1.49
BQ	2	−20.90	−12.53	0.22	−0.83	−2.16	−0.93	−1.74
2MeQ	2	−22.80	−13.75	0.23	−1	−2.34	−1.10	−1.94
NQ	2	−16.70	−12.28	0.38	−1.09	−2.28	−1.15	−1.82

[a] Stoichiometry identified using DFT calculations. [b] ΔG values in kcal mol^{-1}. [c] The experimental ΔG_{bind} was obtained using the stoichiometry identified by DFT and corroborated through function fitting. [d] Experimental uncertainty in ΔG_{bind} was propagated from the uncertainty in K from the function fits. [e] *vs.* Fc/Fc^+. [f] Experiments suggest that the there is no measurable binding between the DDQ^{2-} dianion and CO_2. [g] The calculated binding energy for the DDQ^{2-} is reported for the first binding.

(eqn (1)). The radical anion then undergoes reduction to the dianion, Q^{2-} (eqn (2)), which then binds n CO_2 molecules, as represented in eqn (3). The two reversible single-electron reduction features associated with eqn (1) and (2) are well known for quinones in aprotic solvents in the absence of electrophiles such as CO_2.[12,18,19] Furthermore, we posit that CO_2 binding (eqn (3)) occurs primarily after the second reduction due to the observed lack of a shift in the potential of the first reduction for all quinones studied herein. Although previous studies have found evidence for binding of CO_2 to the semiquinone radical anion,[20] the contribution of these species to CO_2 binding is negligible relative to that of the dianion, and thus is not expected to significantly affect the calculated values for the free energy of CO_2 binding. Due to spectrochemical evidence for stepwise CO_2 binding to reduced quinones species, we propose that stepwise addition is most likely.[14] As such, experimental K values describe a single CO_2 addition reaction (in the case of $n = 1$) or the sum of two stepwise CO_2 additions that sum to eqn (3) (in the case of $n = 2$).

Next, we consider the equilibria and Nernstian relationships governing the reactions and the electrochemical potentials at which they are observed. The half-wave potential for a given redox couple is given by the Nernst equation, eqn (4):

$$E_{\frac{1}{2}} = E^{\circ}_{\frac{1}{2}} - \frac{RT}{zF}\ln\left(\frac{[\mathrm{Red}]}{[\mathrm{Ox}]}\right) \quad (4)$$

Here $E_{\frac{1}{2}}$ is the observed half-wave potential, $E^{\circ}_{\frac{1}{2}}$ is the standard half-wave potential, R is the gas constant, T is the temperature in Kelvin, z is the number of electrons transferred in the redox process, F is the Faraday constant, [Red] is the concentration of the reduced species, and [Ox] is the concentration of the oxidized species.

Because CO_2 binding is both observed electrochemically and predicted by DFT to occur after the second reduction (described by eqn (2), the number of electrons transferred is one (*i.e.* $z = 1$). Additionally, the reduced species is Q^{2-}(*i.e.* $[\mathrm{Red}] = [Q^{2-}]$) and the oxidized species is $Q^{\bullet-}$ (*i.e.* $[\mathrm{Ox}] = [Q^{\bullet-}]$). As Q^{2-} binds CO_2, the ratio [Red]/[Ox] inside the logarithmic term of eqn (4) decreases. Thus, if the reaction in eqn (3) described by equilibrium constant K occurs sufficiently rapidly for the timescale of the CV, we expect to see a shift in half-wave potential $\Delta E_{\frac{1}{2}}$ upon introduction of CO_2 that increases in magnitude with stronger binding to CO_2. This shift in potential is described by eqn (5):

$$\Delta E_{\frac{1}{2}} = -\frac{RT}{F}\ln\left(\frac{[Q^{2-}]}{[Q^{\bullet-}]}\right) \quad (5)$$

The relationships between the concentrations of the oxidized and reduced species are described by eqn (6)–(8). At equilibrium,

$$K = \frac{\left[\left(Q(CO_2)_n\right)^{2-}\right]}{[Q^{2-}][CO_2]^n} \quad (6)$$

and therefore,

$$[(Q(CO_2)_n)^{2-}] = K[Q^{2-}][CO_2]^n. \quad (7)$$

Additionally, at the half-wave potential, the starting oxidized species is half-converted, and so

$$[Q^{\bullet-}] = [Q^{2-}] + [(Q(CO_2)_n)^{2-}]. \quad (8)$$

If the coupled chemical step reaches equilibrium on the timescale of the CV, by combining eqn (7) and (8), we find that

$$[Q^{\bullet-}] = (K[CO_2]^n + 1)[Q^{2-}]. \quad (9)$$

Substituting eqn (9) into eqn (5) and rearranging, we obtain

$$\Delta E_{\frac{1}{2}} = \frac{RT}{F}\ln(K[CO_2]^n + 1) \quad (10)$$

With eqn (10) in hand, values for $\Delta E_{\frac{1}{2}}$ and $[CO_2]$ were calculated for each quinone for CVs taken under 5%, 30%, and 100% CO_2 (Fig. 2). Dissolved CO_2 concentrations were calculated using a Henry's Law method and the local barometric pressure at the time of data collection (see ESI† for details).[21–23]

$\Delta E_{\frac{1}{2}}$ for each data point was obtained by taking the difference between the half-wave potential for the second quinone reduction under Ar and the corresponding value under CO_2. Because the quinone reductions in the presence of CO_2 are not electrochemically reversible, the typical method of determining $E_{\frac{1}{2}}$ (namely, averaging the potentials at which the peak cathodic and anodic currents occur for the feature) is not applicable. Instead, the inflection point of the feature was taken as an approximate $E_{\frac{1}{2}}$ by finding the zero-point of the smoothed

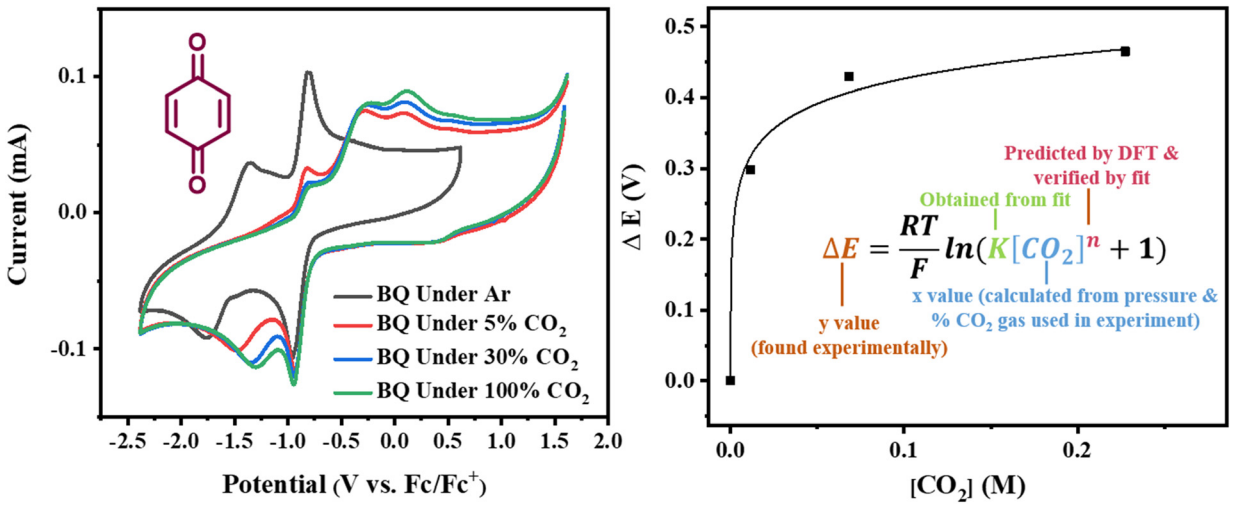

Fig. 2 Left: Cyclic voltammograms of benzoquinone (BQ) under Ar, 5% CO_2, 30% CO_2 and 100% CO_2 taken with a scan rate of 1000 mV s^{-1}. Right: Estimation of CO_2 binding thermodynamics from plots of potential shifts ΔE *vs.* CO_2 concentration [CO_2] through the electrochemical titration of CO_2 and function fitting of eqn (10).

second derivative of the curve, as the inflection point has been previously demonstrated to be a good approximation of $E_{\frac{1}{2}}$.[24]

For quinones with extremely large K values for CO_2 binding (NQ, BQ, and 2MeQ), the peak separation between the first and second reduction features in the CVs becomes minimal. The merging of the two redox waves in the presence of CO_2 renders the inflection point of the second wave difficult to obtain. In these cases, the potential shift for the peak of the feature ΔE_p is taken as an approximation of $\Delta E_{\frac{1}{2}}$. Therefore, the potential values at which the peak current was observed under Ar and under CO_2 were compared to obtain the potential difference. This approximation $\left(\Delta E_p \approx \Delta E_{\frac{1}{2}}\right)$ was tested and found to be reliable for quinones for which both ΔE_p and $\Delta E_{\frac{1}{2}}$ values were readily obtainable. Because separation of the reduction features requires a faster scan rate, these three quinones were given less time to equilibrate with their respective CO_2 adducts over the time course of the CV. Therefore, the K values obtained for these three quinones should be taken as an inherent underestimate (whereas the obtained ΔG is an overestimate, *i.e.* less negative than the true value).

Once values for [CO_2] and $\Delta E_{\frac{1}{2}}$ (or ΔE_p) were obtained for each data point, a plot of [CO_2] *vs.* $\Delta E_{\frac{1}{2}}$ was constructed for each quinone. A user-defined fit function in Origin 2019b was used to determine a best-fit curve with free parameter K based upon eqn (10). The value of n in this equation was defined for each quinone on the basis of DFT results for the favorability of the first and second CO_2 binding events. In the case of quinones with ambiguous DFT binding free energies, n values were determined by comparison of experimental fits with n = 1 and n = 2. Finally, with K values determined for each quinone, the free energy of CO_2 binding, ΔG_{bind}, was calculated using the well-known relationship given by eqn (11).

$$\Delta G_{bind} = -RT\ln(K) \quad (11)$$

Data obtained from experiment was compared with DFT-computed results and is summarized in Table 1.

Results and discussion

The doubly reduced forms of 2MeQ, NQ and BQ, the three electron-rich quinones in the list, bind CO_2 strongly. They were all found to bind two CO_2 units, consistent with literature precedent.[25] Not only are they strong binders of CO_2, but the kinetics of the process are predicted by DFT to be fast with barriers of only 2.4, 4.4, and 5.6 kcal mol^{-1}, respectively, for the first CO_2 binding (Table 2). The second CO_2 binding event is similarly rapid for all three quinones, with barriers of 3.2, 6.1, and 5.1 kcal mol^{-1}, respectively. In fact, the binding of these quinones is so strong and rapid that in order to observe two separate reduction features by CV, scan rates of 300 to 1000 mV s^{-1} were required. The systematic underestimate of binding strength is corroborated by the DFT-computed values of ΔG_{bind}, which are more negative than the experimental values by a larger margin than that of the electron-poor quinones.

For the electron-poor quinones in the series, 2ClNQ, 2ClQ, and 4ClQ, the calculated free energies of binding are in close agreement with the experimental values. A peculiar observation about 2ClQ is that although it falls in the electron-poor category, it binds two equivalents of CO_2. This observation is corroborated experimentally, with fit functions utilizing two equivalents of CO_2 (n = 2) yielding better fit results (Fig. S2.4 and S2.5, ESI†). The final electron-poor quinone, DDQ, was found experimentally to exhibit minimal binding to CO_2, without observable shift in E_{red2} (Fig. S2.8, ESI†), which is consistent with the unfavorable endergonic free energy predicted by DFT. Although in principle a fraction of DDQ may bind CO_2 at high concentrations due to the relatively small positive value of the

Table 2 DFT-computed thermodynamic and kinetic data obtained using the MN15/6-311+G(d,p) level of theory coupled with the SMD solvation model to account for acetonitrile solvent effects. ΔG_{total} is the free energy of binding the first and second CO_2 molecules. Binding and Release $\Delta G^{\ddagger}$ are the activation free energies for the forward and reverse reactions, respectively, as depicted in Scheme 1. All energies are reported in kcal mol^{-1}

	ΔG_{bind}			Binding $\Delta G^{\ddagger}$		Release $\Delta G^{\ddagger}$	
Molecule	1st CO_2	2nd CO_2	ΔG_{total}	1st CO_2	2nd CO_2	1st CO_2	2nd CO_2
DDQ	3.1	11.3	14.4	7.8	12.8	4.7	1.5
4ClQ	−4.9	4.5	−0.5	5.1	8.3	10.0	3.8
2ClQ	−9.8	0.9	−8.9	4.1	6.8	13.9	5.9
2ClNQ	−8.8	1.8	−7.0	4.9	8.2	13.7	6.3
BQ	−15.1	−5.8	−20.9	5.6	5.1	20.7	10.9
2MeQ	−16.8	−5.9	−22.8	2.4	3.2	19.3	9.1
NQ	−13.7	−2.9	−16.7	4.4	6.1	18.2	9.0

free energy of binding, our results indicate that binding was too weak under experimental conditions to quantify even with $n = 1$.

Finally, the CO_2 binding behavior of 4ClQ is of particular interest. With a second reduction potential of −1.18 V *vs.* Fc/Fc$^+$ in dry acetonitrile (positive of the observed reduction potential of O_2 in dry acetonitrile, −1.23 V *vs.* Fc/Fc$^+$),[26] 4ClQ is the only quinone studied which avoids O_2 reduction while still exhibiting CO_2 binding as predicted by DFT and observed experimentally (Table 1 and Fig. S2.6, ESI†). Although the binding free energy of 4ClQ is not as strong as that of the electron-rich quinones, this suggests that quinones with reduction potentials similar to 4ClQ may be in an optimal range for applications in which complete scrubbing of CO_2 is not required. CV can be used to identify quinones of desired ΔG_{bind} through the correlation between their second reduction potential and CO_2 binding strength, as presented in Fig. 3.

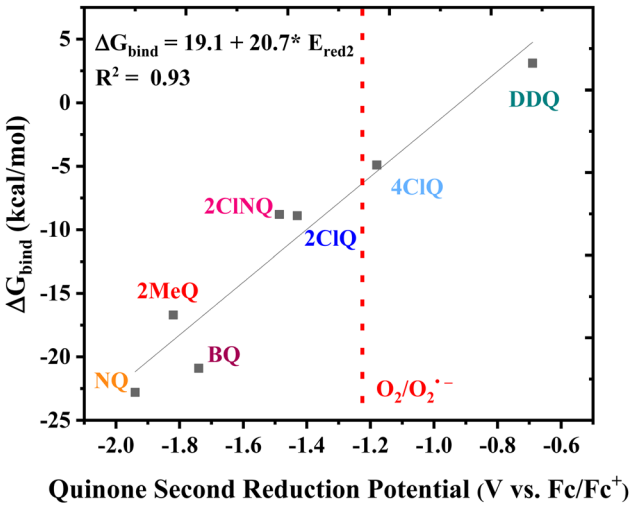

Fig. 3 Linear correlation between the DFT-calculated free energy of CO_2 binding and the experimental second reduction potential of the family of quinones in Fig. 1. The dashed line indicates the approximate potential of O_2 reduction in dry acetonitrile for comparison.

DFT and MK model

Our calculations, summarized in Table 2, indicate that 2ClQ and 2ClNQ are moderate CO_2 binders, with favorable binding of 1 CO_2 and thermoneutral binding of the subsequent CO_2. DDQ and 4ClQ are weak binders as they have less favorable binding of the first CO_2 and endergonic binding of the second CO_2, accompanied by slightly larger activation free energies. Lastly, BQ, NQ and 2MeQ are predicted to be very strong binders, with sequential exergonic CO_2 binding steps and small forward reaction barriers. As such, we expect them to consistently bind 2 CO_2 molecules, in agreement with experiment.

Next, we built a microkinetic model based on DFT-computed thermodynamics (ΔG^0_{bind}) and kinetics ($\Delta G^{\ddagger}_{bind}$) to calculate the weighted stoichiometry of CO_2 molecules per sorbent molecule. This analysis is performed by solving for equilibrium concentrations of A [Q^{2-}], B [$Q(CO_2)^{2-}$], and C [$(Q(CO_2)_2)^{2-}$], for the reactions displayed in Scheme 1 and described in eqn (12)–(20).

Equilibrium concentrations are obtained by solving a system of differential equations describing the rates of formation and degradation of each complex, as described by eqn (12)–(14).

$$\frac{d[A]}{dt} = -r_1 + r_2 \quad (12)$$

$$\frac{d[B]}{dt} = (r_1 + r_4) - (r_2 + r_3) \quad (13)$$

$$\frac{d[C]}{dt} = r_3 - r_4 \quad (14)$$

The forward reactions describing the binding of the 1st and 2nd CO_2 molecules are treated as bimolecular reactions. The rates r_1 and r_3, respectively, depend on the concentrations of the quinone complex as well as that of solvated CO_2:

$$r_1 = k_1[A][CO_2] = \nu \exp\left(-\frac{\Delta G_1^{\ddagger}}{k_B T}\right)[A][CO_2] \quad (15)$$

$$r_3 = k_3[B][CO_2] = \nu \exp\left(-\frac{\Delta G_3^{\ddagger}}{k_B T}\right)[B][CO_2] \quad (16)$$

On the other hand, the reverse reactions describing CO_2 release are unimolecular as the reactant in this case decomposes into a dianion quinone and a solvated CO_2. Rates of CO_2 release are thus not dependent on solvated CO_2 concentrations:

$$r_2 = k_2[B] = \nu \exp\left(-\frac{\Delta G_2^{\ddagger}}{k_B T}\right)[B] \quad (17)$$

$$r_4 = k_4[C] = \nu \exp\left(-\frac{\Delta G_4^{\ddagger}}{k_B T}\right)[C] \quad (18)$$

Finally, to maintain a mass balance, we assume the sum of concentrations of A, B and C, is always equivalent to the concentration of starting material Q^{2-}, which for this study is set to 0.001 M to match experimental conditions.

$$[A] + [B] + [C] = 0.001\ M \quad (19)$$

Section S3 of the ESI† provides further details on this system of differential equations. Equilibrium concentrations are then

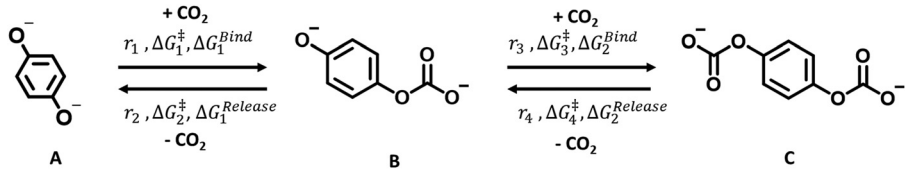

Scheme 1 Overall reaction equilibrium between A, B, and C.

analyzed using eqn (20) to determine the weighted stoichiometry of CO_2 molecules captured at equilibrium, where the ratio $\frac{CO_2}{Q^{2-}}$ yields a value between 0 and 2.

$$\frac{CO_2}{Q^{2-}} = \frac{0 \cdot [A] + 1 \cdot [B] + 2 \cdot [C]}{[A] + [B] + [C]} \quad (20)$$

Fig. 4 demonstrates the ratio $\frac{CO_2}{Q^{2-}}$ for all 7 quinones investigated at 4 varying concentrations of solvated CO_2, ranging from 10^{-5} M to 0.3 M. In agreement with experiment (Table 1), our model predicts that BQ, NQ, and 2MeQ are very strong CO_2 binders, averaging a 2 : 1 stoichiometry of CO_2 per Q^{2-} dianion across experimentally relevant concentrations of CO_2 ($0.01\ M < [CO_2] < 0.3\ M$). This results from sequentially exergonic CO_2 binding thermodynamics and small reaction barriers, as shown in Table 2. The moderate binders – 2ClQ and 2ClNQ – also have a weighted $\frac{CO_2}{Q^{2-}}$ stoichiometry closer to 2 : 1 at high CO_2 concentrations, although the stoichiometry drops at smaller $[CO_2]$ values. This indicates that moderate binders favor the binding of only one CO_2 molecule at lower concentrations, as expected from computed ΔG_{bind} values that are exergonic for the 1st CO_2 binding step and only slightly more positive than thermoneutral for the second CO_2 binding step. 4ClQ maintains a $\frac{CO_2}{Q^{2-}}$ ratio of $\sim$1 that increases gradually as the CO_2 saturation limit is approached, as depicted in

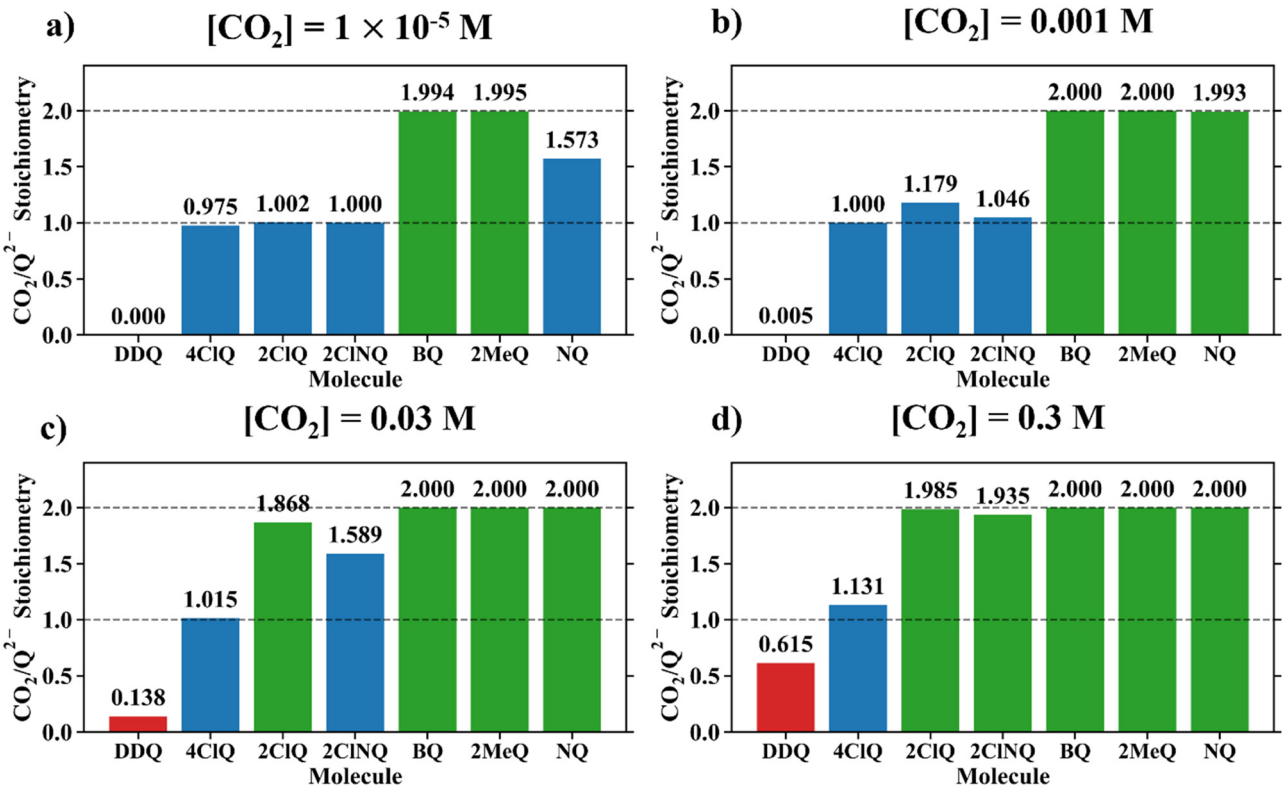

Fig. 4 CO_2 stoichiometry relative to Q^{2-} evaluated using eqn (20) at (a) $[CO_2] = 10^{-5}$ M, (b) $[CO_2] = 0.001$ M, (c) $[CO_2] = 0.03$ M, and (d) $[CO_2] = 0.3$ M, assuming the starting concentration for $[Q^{2-}] = 0.001$ M. The model is representative of the dataset obtained using the MN15/6-311+G(d,p) level of theory with acetonitrile solvation as described by the SMD implicit solvent model.[27–30] 0.3 M of CO_2 is the saturation limit in acetonitrile.[21] 3 classes of binders can be specified based on this data – strong binders (Q, NQ, and 2MeQ), moderate binders (2ClNQ and 2ClQ), and weak binders (4ClQ and DDQ). Strong binders are generally insensitive to $[CO_2]$ across 5 orders of magnitude, as they consistently bind 2 CO_2 molecules. Moderate and weak binders are sensitive to CO_2 concentrations, as moderate binders produce a stoichiometry range of 1 to 2 and weaker binders a stoichiometry range of 0 to 1 across the examined range of CO_2 concentrations.

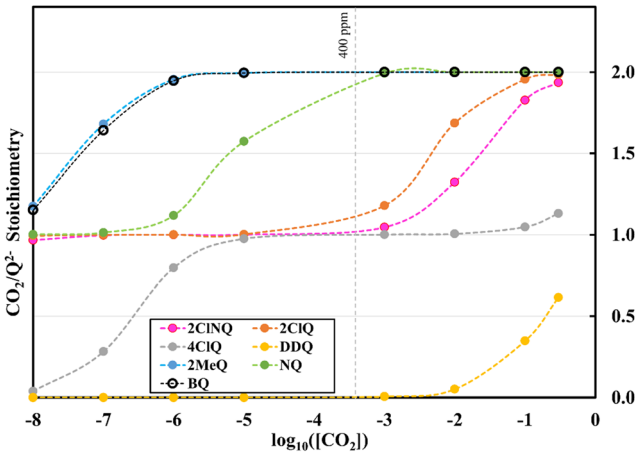

Fig. 5 CO_2 stoichiometry relative to Q^{2-} as a function of CO_2 concentration in logarithmic scale. Stoichiometry values are obtained by solving the system of differential equations (eqn (12)–(20)) at varying CO_2 concentrations. CO_2 concentrations in our analyses span 8 orders of magnitude, ranging from 10^{-8} M to 0.3 M. The vertical dashed grey line represents atmospheric concentration of ~400 ppm.

Fig. 4d. DDQ is mostly unreactive, however higher concentrations of CO_2 push the 1st CO_2 binding step forward to some extent, resulting in a value of $\frac{CO_2}{Q^{2-}} = 0.615$ at the saturation limit.

To further illustrate the dependence of the calculated weighted stoichiometry $\frac{CO_2}{Q^{2-}}$ on CO_2 concentrations, we plot $\frac{CO_2}{Q^{2-}}$ as a function of $\log[CO_2]$, as shown in Fig. 5. This enables the analysis of the dependence $[CO_2]$ over the span of 8 orders of magnitude for all 7 quinones in our study. We find that the weighted stoichiometry of strong binders falls for $[CO_2] < 10^{-5}$ M. This suggests that their efficiency as sorbents is independent of CO_2 concentration at atmospheric concentrations (415 ppm) or higher. The moderate binders – 2ClQ and 2ClNQ – are strongly dependent on CO_2 concentration at high values ($[CO_2] > 10^{-4}$ M), whereas at lower CO_2 concentrations they exhibit a $\frac{CO_2}{Q^{2-}}$ stoichiometry value of 1. As such, unlike the strong binders, the carbon capture efficiency of the moderate binder quinones benefit from higher CO_2 concentrations. 4ClQ appears to be only dependent on $[CO_2]$ at extremely low or extremely high concentrations. DDQ is generally unreactive unless the solvent is saturated with CO_2.

Conclusions

As previously observed for a family of C-nucleophiles,[10] we now report a linear correlation between the potential required to generate quinone dianions and their free energy of CO_2 binding. Unlike the relatively simple electrogenerated C-nucleophiles of our previous report, the doubly reduced quinones exhibit variable stoichiometric coefficients when binding to CO_2. This observation has direct implications for the development of O_2-impervious quinone molecular sorbents, where maximal CO_2 loading is sought. Our findings suggest that CO_2-reactive quinone dianions can in fact be generated at potentials more positive than oxygen reduction. However, in some cases, such dianions have a binding stoichiometry of 1 : 1 rather than the previously observed stoichiometry CO_2/Q^{2-} of 2 : 1 for well-studied, electron-rich quinones such as NQ. This experimental observation is corroborated by DFT-computed thermodynamics and kinetics. The calculations inform a microkinetic model and validate the variability in quinone behavior at different concentrations of CO_2. Moderate and weak CO_2 binders exhibit CO_2/Q^{2-} stoichiometries that vary between 0 and 2, depending on CO_2 concentration, whereas strong binders are not as sensitive to CO_2 concentrations and maintain a CO_2/Q^{2-} stoichiometry of 2 : 1 across CO_2 concentrations for $[CO_2] > 10$ ppm. The sensitivity of chemical equilibrium to CO_2 concentration indicates that strong quinones do not require higher CO_2 concentrations to bind 2 CO_2 molecules, whereas moderate binders (*e.g.* 2ClNQ and 2ClQ, whose values for ΔG_{bind} fall between −5 and −10 kcal mol^{-1}) benefit from higher CO_2 concentrations as their weighted stoichiometries increase substantially from ~1 : 1 at atmospheric concentrations to ~2 : 1 near the saturation limit. Synergistic theoretical and experimental results indicate that one quinone studied, 4ClQ, exhibits reduction potentials positive of O_2/O_2^- while still binding CO_2 sufficiently strongly for an average of one CO_2 bound per quinone even at low CO_2 concentrations. Combined with careful consideration of the lower CO_2 capacity of 1 : 1 stoichiometry and the predictive ability of the correlation, this observation could allow for facile identification of other O_2-impervious quinones capable of binding CO_2. Using simple electrochemical measurements, the correlation between reduction potential and CO_2 binding strength can be used to predict carbon capture performance of new molecular materials in the quinoid family. Based on our findings, binding stoichiometry varies depending on assay conditions.

Conflicts of interest

The authors declare no competing interests.

Acknowledgements

We thank Prof. Carl Koval, and Prof. Rich Noble for useful discussions. ORL thanks the University of Colorado for startup funds. HP thanks the University of Colorado Department of Chemistry for a summer 2021 research fellowship and the National Science Foundation Graduate Research Fellowship Program. AWH acknowledges support from a fellowship provided by Kuwait University. This material is based upon work supported by the National Science Foundation Graduate Research Fellowship under Grant No. DGE 2040434. SNS would like to acknowledge the University of Colorado Boulder UROP program.

References

1 S. Fuss, J. G. Canadell, P. Ciais, R. B. Jackson, C. D. Jones, A. Lyngfelt, G. P. Peters and D. P. Van Vuuren, *One Earth*, 2020, **3**, 145–149.
2 C. Koven, V. K. Arora, P. Cadule, R. A. Fisher, C. D. Jones, D. M. Lawrence, J. Lewis, K. Lindsey, S. Mathesius and M. Meinshausen, *Earth Syst. Dyn. Discuss.*, 2021, 1–32.
3 J. Wilcox, *Nat. Energy*, 2020, **5**, 121–122.
4 J. Wilcox, *Carbon capture*, Springer Science & Business Media, 2012.
5 C. Hou, D. R. Kumar, Y. Jin, Y. Wu, J. J. Lee, C. W. Jones and T. Wang, *Chem. Eng. J.*, 2021, **413**, 127532.
6 H. A. Petersen and O. R. Luca, *Phys. Chem. Chem. Phys.*, 2021, **23**, 12533–12536.
7 P. Scovazzo, J. Poshusta, D. DuBois, C. Koval and R. Noble, *J. Electrochem. Soc.*, 2003, **150**, D91.
8 S. Voskian and T. A. Hatton, *Energy Environ. Sci.*, 2019, **12**, 3530–3547.
9 F. Simeon, M. C. Stern, K. M. Diederichsen, Y. Liu, H. J. Herzog and T. A. Hatton, *J. Phys. Chem. C*, 2022, **126**, 1389–1399.
10 H. A. Petersen, A. W. Alherz, T. A. Stinson, C. G. Huntzinger, C. B. Musgrave and O. R. Luca, *iScience*, 2022, **25**, 103997.
11 B. Gurkan, F. Simeon and T. A. Hatton, *ACS Sustainable Chem. Eng.*, 2015, **3**, 1394–1405.
12 M. E. Peover and J. D. Davies, *J. Electroanal. Chem.*, 1963, **6**, 46–53.
13 C. Creutz, *Electrochemical and Electrocatalytic Reactions of Carbon Dioxide*, Elsevier, 1993, pp. 19–67.
14 A. M. D. L. DuBois, W. Bell and J. C. Smart, in *Electrochemical and Electrocatalytic Reactions of Carbon Dioxide*, ed. K. K. B. P. Sullivan, and H. E. Guard, Elsevier, Amsterdam, 1993.
15 T. Nagaoka, N. Nishii, K. Fujii and K. Ogura, *J. Electroanal. Chem.*, 1992, **322**, 383–389.
16 N. Gupta and H. Linschitz, *J. Am. Chem. Soc.*, 1997, **119**, 6384–6391.
17 J. M. Barlow and J. Y. Yang, *J. Am. Chem. Soc.*, 2022, **144**, 14161–14169.
18 M. E. Peover, *J. Chem. Soc. (Resumed)*, 1962, 4540, DOI: **10.1039/jr9620004540**.
19 M. T. Huynh, C. W. Anson, A. C. Cavell, S. S. Stahl and S. Hammes-Schiffer, *J. Am. Chem. Soc.*, 2016, **138**, 15903–15910.
20 M. B. Mizen and M. S. Wrighton, *J. Electrochem. Soc.*, 1989, **136**, 941–946.
21 A. Gennaro, A. A. Isse and E. Vianello, *J. Electroanal. Chem. Interfacial Electrochem.*, 1990, **289**, 203–215.
22 M. B. Ewing and J. C. S. Ochoa, *J. Chem. Eng. Data*, 2004, **49**, 486–491.
23 National Center for Atmospheric Research Lab, NCAR Foothills Lab Weather, NCAR, Boulder, CO.
24 E. M. Espinoza, J. A. Clark, J. Soliman, J. B. Derr, M. Morales and V. I. Vullev, *J. Electrochem. Soc.*, 2019, **166**, H3175–H3187.
25 S. Voskian and T. A. Hatton, *Energy Environ. Sci.*, 2019, **12**, 3530–3547.
26 M. Zimmermann, *Oxygen reduction reaction mechanism on glassy carbon in aprotic organic solvents*, Doctoral dissertation, Université Grenoble Alpes (ComUE), 2015.
27 H. S. Yu, X. He, S. L. Li and D. G. Truhlar, *Chem. Sci.*, 2016, **7**, 5032–5051.
28 D. Andrae, U. Häußermann, M. Dolg, H. Stoll and H. Preuß, *Theor. Chim. Acta*, 1990, **77**, 123–141.
29 M. J. Frisch, G. W. Trucks, H. B. Schlegel, G. E. Scuseria, M. A. Robb, J. R. Cheeseman, G. Scalmani, V. Barone, G. A. Petersson, H. Nakatsuji, X. Li, M. Caricato, A. V. Marenich, J. Bloino, B. G. Janesko, R. Gomperts, B. Mennucci, H. P. Hratchian, J. V. Ortiz, A. F. Izmaylov, J. L. Sonnenberg, D. Williams-Young, F. Ding, F. Lipparini, F. Egidi, J. Goings, B. Peng, A. Petrone, T. Henderson, D. Ranasinghe, V. G. Zakrzewski, J. Gao, N. Rega, G. Zheng, W. Liang, M. Hada, M. Ehara, K. Toyota, R. Fukuda, J. Hasegawa, M. Ishida, T. Nakajima, Y. Honda, O. Kitao, H. Nakai, T. Vreven, K. Throssell, J. A. Montgomery Jr., J. E. Peralta, F. Ogliaro, M. J. Bearpark, J. J. Heyd, E. N. Brothers, K. N. Kudin, V. N. Staroverov, T. A. Keith, R. Kobayashi, J. Normand, K. Raghavachari, A. P. Rendell, J. C. Burant, S. S. Iyengar, J. Tomasi, M. Cossi, J. M. Millam, M. Klene, C. Adamo, R. Cammi, J. W. Ochterski, R. L. Martin, K. Morokuma, O. Farkas, J. B. Foresman and D. J. Fox, *Gaussian 16*, 2016.
30 A. Marenich, C. Cramer and D. Truhlar, *J. Phys. Chem. B*, 2009, **113**, 6378.